Proceedings of the ASME 2010 3rd Joint US-European Fluids Engineering Summer Meeting and 8th International Conference on Nanochannels, Microchannels, and Minichannels
FEDSM-ICNMM2010
August 1-5, 2010, Montreal, Canada

FEDSM-ICNMM2010-30651

ANALYSIS OF AXIAL MENISCUS JUMP-LIKE TRANSITION IN RECTANGULAR MICROGROOVES

Chaohong Guo / Institute of Engineering Thermophysics, CAS/guochaohong@mail.etp.ac.cn

Xuegong Hu / Institute of Engineering Thermophysics, CAS / xuegonghu@mail.etp.ac.cn

Tao Wang / Institute of Engineering Thermophysics, CAS / wangtao@mail.etp.ac.com

Dawei Tang / Institute of Engineering Thermophysics, CAS / dwtang@mail.etp.ac.cn

ABSTRACT

The meniscus receding process was studied for the axial steady flow in open rectangular microgrooves based on experimental results. Experimental results show that the liquid film recedes remarkably as a cubic trendline from the accommodation stage to the bottom corner-flow stage, but the dead zone and the step change don't exist. The receding process of the liquid film between the accommodation stage and the bottom corner-flow stage is named jump-like transition in the paper. Characteristics of the axial flow in rectangular microgrooves were theoretically analyzed considering the meniscus receding performance in the jump-like transition, calculation results show that radius of the meniscus curvature decreases along the groove axis, which provides drive for the axial flow; the liquid cross sectional area and the liquid height decrease evidently at the stage of the jump-like transition; the liquid velocity increases along the axis, and increases promptly at the transition stage and the corner flow stage.

INTRODUCTION

Capillary microgroove can drive fluid flow by capillary force and create enhanced phase-change heat transfer conditions by promoting the formation of an extended meniscus adjacent to the triple phase contact line [1~5]. The heat sink with capillary microgrooves has the strong potential to achieve efficient heat exchanges with high heat transfer coefficients and heat fluxes, and it is capable to be used in spacecraft thermal control, high-power laser thermal management and microelectronic device cooling system.

A number of investigations have been conducted in triangular grooves by now. Ayyaswamy et al. [6] indicated that the friction factor depends on shape of triangular microgrooves and contact angle of fluids. Ha & Peterson predicted the axial dryout point for evaporating liquids in triangular microgrooves [7~10]. Catton & Stroes [11] considered the accommodation stage, and established a semi-analytical model to predict the capillary limit of inclined triangular grooves.

A triangular groove provides only half the cross sectional area of a rectangular groove with the same groove width and height, and the viscous friction is greater, reducing the axial flow rate [12-14]. Thus, the rectangular groove has vast application potentials. Only few studies have been made on rectangular grooves by now. Stroes & Catton[15] indicated that the rectangular groove is liquid-full at its inlet and an accommodation region or meniscus deformation region exists wherein the meniscus remains attached to the upper corners of the groove as it adjusts from its inlet configuration to the smaller values associated with the minimum contact angle adjusted for local evaporation. Nilson et al [14] analyzed axial flow characteristics of rectangular grooves and divided the axial flow into two stages: the accommodation stage (meniscus deformation stage), and the corner flow stage, as seen in Fig. 1. Nilson et al [14] proposed that the meniscus steeply jumps down to the groove bottom at the end of the accommodation stage because the meniscus curvature radius can't become smaller at this point. After the step change, corner flow occurs wherein radius of the meniscus curvature decreases continually. To our knowledge, the dead zone is assumed just for simplifying theoretical analyses and it does not exist in fact, the meniscus has to recede gradually until touches the groove bottom but not jumps down steeply from the accommodation stage to the corner flow stage. By now, there have been few experimental results that verify the meniscus receding profile, and no desirable theoretical model intents to analyze the meniscus jump-like transition.

The present paper originally analyzes the meniscus jump-like transition based on experimental results, and describes the meniscus receding profile in rectangular microgrooves. The paper offers novel and meaningful results for further research on flow characteristics in rectangular microgrooves.

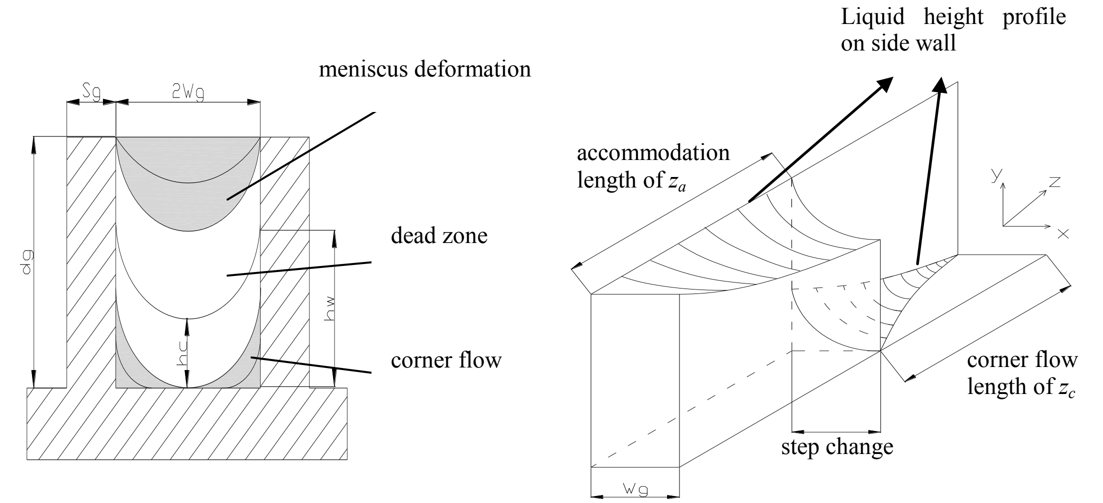

(a) Liquid configuration in rectangular microgroove (b) Schematic of axial flow along rectangular microgroove

Fig. 1 Meniscus distribution in rectangular microgroove proposed by Nilson et al [14]

NOMENCLATURE

Symbol	Description	Unit
A_L	area of liquid cross section	m^2
d_g	microgroove depth	m
F_V	friction pressure resistance	N
h_c	central height of liquid film	m
h_w	liquid height on side wall	m
h_{fg}	latent heat	kJ/kg · K
$\dot{m}$	liquid mass flow rate	kg/s
p_L	liquid pressure	Pa
p_V	vapor pressure	Pa
q	heat flux	kw/m^2
r	radius of meniscus curvature	m
s_g	microgroove pitch	m
u_V	axial velocity	m/s

Symbol	Description	Unit
w_g	microgroove width	m
z_a	accommodation length	m
z_b	axial length of jump-like transition	m
z_c	axial length of corner flow	m
z'	observed wetting length in heating zone	m
	Greek symbols	
β	friction factor	
μ_L	liquid viscosity	kg/ms
ρ_L	liquid density	kg/m^3
α	surface tension	N/m
θ	angle of slop of the plate	

THEORETICAL MODEL FOR AXIAL FLOW IN RECTANGULAR GROOVES

The liquid film, driven by axial gradient of capillary pressure, overcomes the gravity and flows along inclined rectangular grooves. The general form of the force-momentum balance equation can be expressed as:

$$\rho\left[\partial u/\partial t + \left(u\cdot\nabla\right)u\right] = -\nabla P + F + \mu\nabla^2 u \qquad (1)$$

Some reasonable assumptions are introduced in the axial flow model for simplifying theoretical analyses: 1. The convective term in the governing equation (1) can be neglected because the flow in microgrooves is very slow; 2. The liquid flow in microgrooves is steady laminar flow; 3. At the accommodation stage, radius of the meniscus curvature is constant and the meniscus is in the shape of circular arc on the cross section since the Bond number *Bo* is usually small in channels with submillimeter width [14]; 4. On the cross section, the contact angle between the liquid and the wall is assumed as 0°.

Based on the assumption of '2", the force-momentum equation can be simplified as:

$$\frac{dp_L}{dz} + \rho_L g \sin\theta + F_V = 0 \qquad (2)$$

(1) Accommodation stage

Applying the Young-Laplace equation: $p_V - p_L \approx \sigma/r(z)$, Eq. (2) can be expressed as:

$$\frac{d}{dz}\left(\frac{\sigma}{r(z)}\right) = \frac{\beta\dot{m}\mu_L}{4{w_g}^2 A_L \rho_L} + \rho_L g \sin\theta \qquad (3)$$

The parameter β is simply the reciprocal of the normalized mean fluid speed, U^*, defined in $\beta = 1/U^*$ by Tchikanda et al [16]. This expression is based upon blending of analytical results that apply in asymptotic limits of fluid depth and contact angle, with the blending parameters chosen to obtain best agreement with detailed numerical solutions [16].

Geometrical parameters in Eq. (3) can be expressed as:

$$h_c = d_g - r + \sqrt{r^2 - w_g^2} \qquad (4)$$

$$A_L = 2w_g(h_c + r_{\min}) + (d_g - h_c + r)w_g - (\pi/2 - \arccos w_g/r)r^2 \qquad (5)$$

Boundary conditions of the accommodation stage are defined in Eq. (6). The minimal radius of the meniscus curvature is half of the groove width if the minimal contact angle is 0^o.

$$z=0 \qquad r=\infty; \qquad z=z_a \qquad r=w_g \qquad (6)$$

（2）Corner flow stage

The liquid continues to recede into two identical triangular grooves after touching bottom of the rectangular groove. The momentum equation for liquid flow in each triangular groove is similar with Eq. (3) except definition of the mass flow which is discussed later. The friction coefficient β is set to be 93.93 [14], substitution of $\beta=93.93$ into Eq. (3) yields axial flow differential equation for corner flows.

Liquid cross sectional area, A_L, can be expressed as:

$$A_L = r^2 - \pi r^2/4 \qquad (7)$$

Filleted corners always exist at the bottom of the microgroove with fillet radius of r_{min} because of manufacturing tolerance. Boundary conditions of the corner flow stage can be defined in Eq. (8) considering the filleted corners.

$$z=z_a \qquad r=w_g \quad ; \qquad z=z_a+z_c \qquad r=r_{\min} \quad (8)$$

ANALYSIS OF CALCULATION AND EXPERIMENTAL RESULTS

1. Experiment introduction

As seen in Fig. 2 (a) and (b), a transparent boroscilicate plate, on which rectangular microgrooves are machined, is inserted in an ethanol reservoir, a membrane heater adheres to back of the plate and supplies input power through adjusting the DC electrical source. The standard error of the input power is less than ±0.6W. The plate, the reservoir and a cooling water tube are all closed in a transparent container. The liquid in microgrooves absorbs heat and evaporates, and then the vapor is condensed by cooling water tube in the container. As seen in Fig. 2 (b), the plate is uncapped and the microgrooves are open to the container space. Pressure of the container space is measured by an pressure sensor with measurement accuracy of ±0.5%, and one atmosphere pressure is maintained in the container. The plate is 90mm long, 20mm wide and 1mm thick, the angle of slop of the plate is 70^o, the membrane heater with dimension of 10mm×20mm adheres to back of the plate with axial distance of 35mm away from the reservoir. Thermal insulation is used on the back of the plate to prevent heat diffusion. The plate is always processed by ultrasound cleaning before experiment. It must be pointed out that filleted corners exist at the bottom of the groove with fillet radius of $r_{min}\approx 50\mu m$ because of manufacturing tolerance, as seen in Fig. 2 (c). The groove depth of d_g, the central height of liquid film h_c and the liquid height on side wall h_w are defined in Fig. 2 (c).

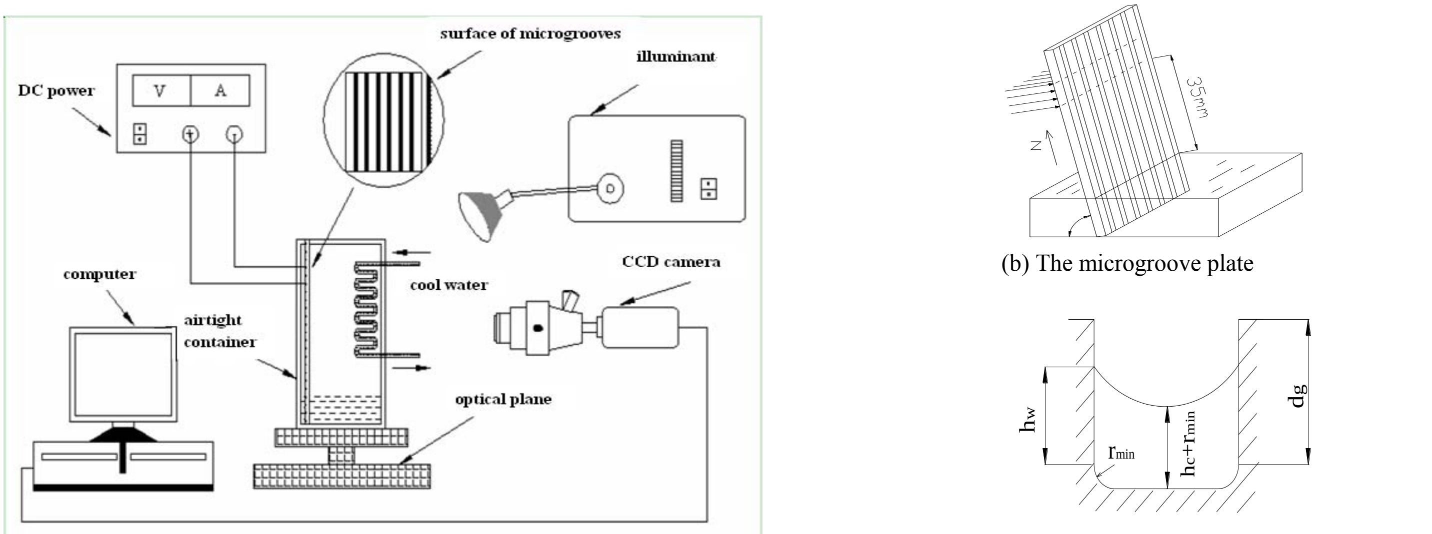

(a) Experimental apparatus

(b) The microgroove plate

(c) Cross section of rectangular groove

Fig. 2 Schematic of the experimental system

Axial flow performance in rectangular microgrooves was observed by a high-speed camera with the maximum speed of 100,000 frames per second, a CCD camera with 5M pixels, and a microscope; thermal field of the plate surface was measured by an infrared thermoviewer. The experimental system has high measurement accuracy and good performance, so it provides reliable information for experimental analyses. The axial profile of h_w in the heating zone was clearly visualized by camera, and then was processed by computer as shown in Fig. 3. Experimental results were got under different conditions, as shown in Table 1. Axial flow characteristics in rectangular microgrooves were analyzed based on these experimental results.

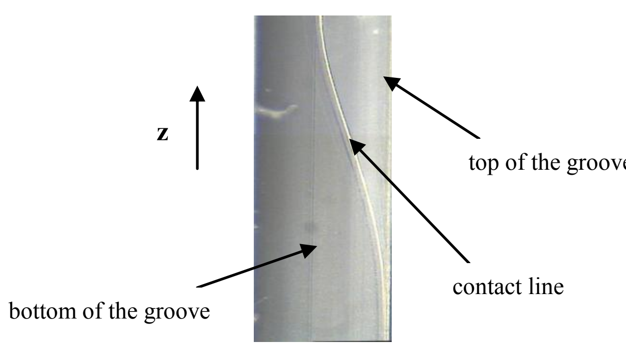

Fig. 3 Liquid height profile on the side wall

Table 1 Experimental conditions

	Groove depth (mm)	Groove width (mm)	Heat flux (kw/m^2)
1	0.4	0.15	17
2	0.4	0.15	30
3	0.4	0.15	38
4	0.5	0.2	17.5
5	0.5	0.3	17.5
6	0.5	0.4	17.5

2 Comparison between calculation and experimental data

Observation shows that the meniscus remains attached to the upper corners of the groove from the reservoir to the heating zone, which associates with the accommodation theory proposed by Stroes & Catton [11, 15] and Nilson et al [14]. According to the experimental observation, the accommodation length can be set 35mm, which is the distance from the reservoir to the heating zone.

The heat diffusion is neglected because of the thermal insulation on the back of the microgrooves. There is no heat load that puts on the accommodation region, so the mass flow rate at the accommodation stage can be shown as follows:

$$\dot{m} = q \cdot (2w_g + s_g) \cdot z' / h_{fg} \qquad (9)$$

Accommodation lengths under different working conditions were concluded by iterative calculation. As shown in Fig. 4, when the groove width is 0.15mm and the depth is 0.4mm, the calculated accommodation lengths are all close to the experimental result of 35mm under different heat load conditions, so the accommodation region can be set from the reservoir surface to the heating zone, the liquid height on the side wall of h_w always equals the groove depth of d_g during the accommodation stage. When the groove width increases, the calculated accommodation length gradually decreases to less than the experimental result of 35mm. Under these conditions, the flow status seems like that: the liquid height of h_w doesn't decrease obviously because there is no heat load in this region and evaporation near the triple-phase contact line is quite weak, but the meniscus can't remain circular and maybe becomes in the shape of parabola or ellipse though it still adheres to the upper corners of the groove. The side liquid height of h_w obviously decreases until the liquid strongly evaporates in the heating zone. The speculation mentioned above is based on the accommodation theory, and further experimental studies, especially observations on the meniscus deformation in cross section, are needed to verify and improve the theoretical analyses.

As seen in Fig. 4, the accommodation length can be set 35mm except for the groove with width of 0.3mm and 0.4mm respectively. Particular analysis is reserved until acquiring richer experimental data for these conditions.

The axial profile of h_w is calculated by the analytical model proposed above when the groove width is 0.15mm, the depth is 0.4mm, and the heat load is 30kw/m^2, and the calculation result is compared with the experimental data.

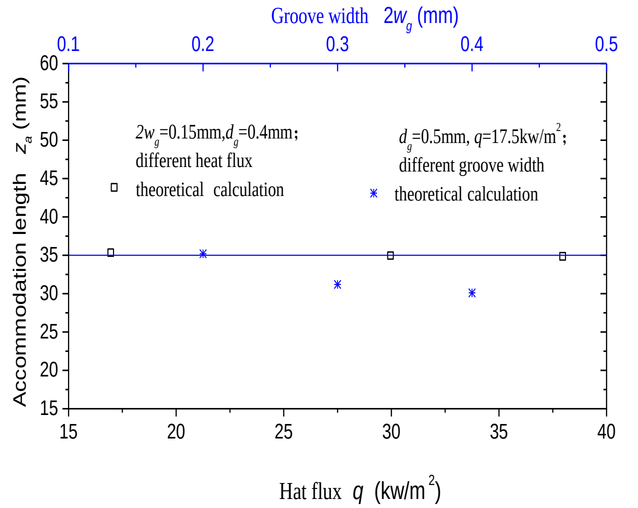

Fig. 4 Accommodation length of z_a under different conditions

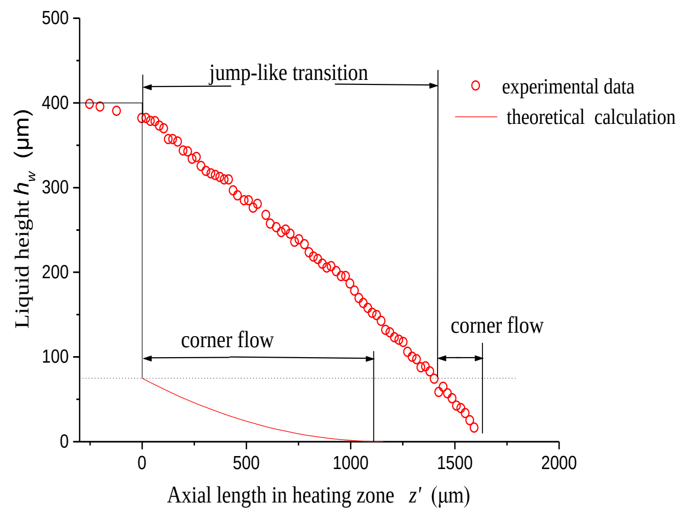

Fig. 5 Comparison of the side liquid height profile in heating zone

The total mass flow rate in the rectangular groove is split in two at the corner flow stage, thus for a single triangular section of the rectangular groove:

$$\dot{m} = 1/2 \cdot q \cdot (2w_g + s_g) \cdot (z - z_a) / h_{fg}$$
$$z_a \le z \le z_a + z_c \qquad (10)$$

The axial profile of h_w was deduced by iterative calculation of Eq. (3), (7), (8), (10); Fig. 5 shows comparison between calculation and experimental data. The experimental curve shows obviously that the meniscus recedes significantly but not steeply jumps down to the bottom of the groove as a step change, so the dead zone and the step change proposed by Stroes & Catton [11, 15] and Nilson et al [14] don't exist in fact. We define the stage of the meniscus receding process between the accommodation stage and the corner flow stage as the jump-like stage. In addition, as seen in Fig. 5, the corner flow distance calculated by the theoretical model is longer than the experimental result, so the calculation underestimates the axial flow resistance at the corner flow stage and a larger friction term is needed.

ANALYSIS OF THE JUMP-LIKE TRANSITION

Experimental results show that the axial profile of h_w is approximately of a cubic polynomial form in the jump-like transition. The profile of h_c can be assumed as shown in Eq. (11) with boundary conditions defined in Eq. (12).

$$h_c = a\cdot z^3 + b\cdot z^2 + c\cdot z + d \qquad (11)$$

$$z = z_a \quad h_c = d_g - w_g;\quad z = z_a + z_b \quad h_c = -r_{\min}$$

$$z = z_a \quad dh_c/dz = g_o;\quad z = z_a + z_b \quad dh_c/dz = g_e \qquad (12)$$

Where z_b equals the axial distance from $h_w=d_g$ to $h_w=w_g$. g_o is axial varying gradient of h_c at the position of $z=z_a$. g_e is axial varying gradient of h_c at the end of the jump-like transition. The beginning of the jump-like transition is in the position of $z=z_a$ where gradients of h_w and h_c should be 0 according to the accommodation theory, but dh_c/dz is not 0 in fact because little axial heat diffusion exists in the plate and then the liquid height profile is influenced. The variable of g_o is adjusted in range of $-\mathrm{tg}0^0 \sim -\mathrm{tg}15^0$ according to experimental data. On the axial section, the contact angle between the liquid and the boroscilicate plate is nearly 10^0 according to the observation, so $g_e=-\mathrm{tg}10^0$ is set. At the stage of the jump-like transition, the radius of the meniscus can be assumed constant and $h_w=h_c+w_g$ can be adopted because of short distance of this stage. The axial profile of h_w can be deduced from the fitting equation (11) of the central liquid height h_c.

Comparisons of the axial profile of h_w between calculation of the fitting equation and experimental data are shown in Fig. 6 and Fig. 7. The axial profiles of h_w are not calculated for the groove with width of 0.3mm and 0.4mm respectively because the accommodation theory is not perfectly applicable and $h_w=h_c+w_g$ cannot be accepted under these conditions. As seen in Fig. 6, the axial flow distance decreases when the heat flux increases since the liquid evaporation becomes stronger for higher heat load. Fig. 6 and Fig. 7 show that the meniscus recedes with a cubic polynomial form, and calculated curves are very close to the experimental data. Coefficients mentioned in Eq. (11) are reasonably adjusted for different dimensions of microgrooves and different heat loads. Further observations are needed to improve the fitting equation (11).

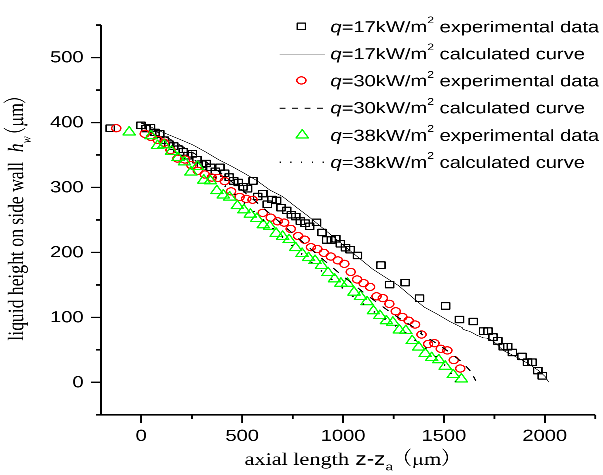

Fig. 6 Comparison between experiment and calculation when $2w_g$=0.15mm and d_g=0.4mm

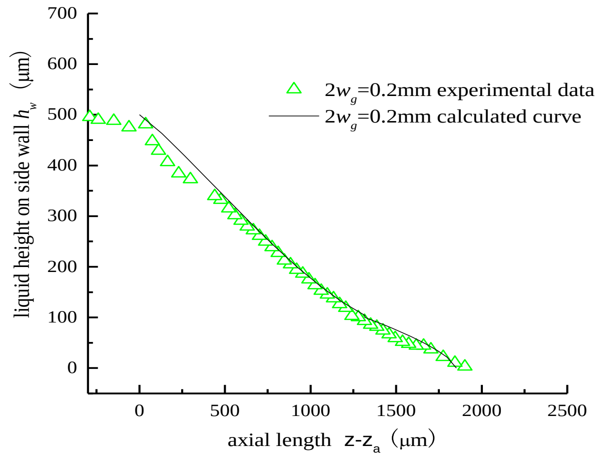

Fig. 7 Comparison between experiment and calculation when $2w_g$=0.2mm, d_g=0.5mm, q=17.5 kw/m^2

At the stage of the jump-like transition, axial change curves of some parameters such as mass flow rate, axial velocity, liquid cross sectional area, etc. can be deduced by iterative calculation of Eq. (3). At the jump-like stage:

$$\dot m = q\cdot(2w_g + s_g)\cdot(z - z_a)/h_{fg} \qquad z_a \le z \le z_a + z_b \qquad (13)$$

$$u = \dot m / (\rho_L A_L) \qquad (14)$$

$$A_L = 2w_g(h_c + r_{\min}) + (h_w - h_c + r)w_g - (\pi/2 - \arccos w_g/r)r^2 \qquad (15)$$

At the corner flow stage, the liquid recedes significantly towards the apex of the groove. According to experimental results, the friction factor of β in Eq. (3) underestimates the friction augmentation caused by small liquid cross sectional area. Therefore, the factor of β is multiplied by C_f which is set in range of 10~15. Considering length of the jump-like transition, the mass flow rate and boundary conditions at the corner flow stage can be expressed as:

$$\dot m = 1/2\cdot q\cdot(2w_g + s_g)\cdot(z - z_a - z_b)/h_{fg}$$

$$z_a + z_b \le z \le z_a + z_b + z_c \qquad (16)$$

$$z = z_a + z_b \qquad r = w_g\ ;$$

$$z = z_a + z_b + z_c \qquad r = r_{\min} \qquad (17)$$

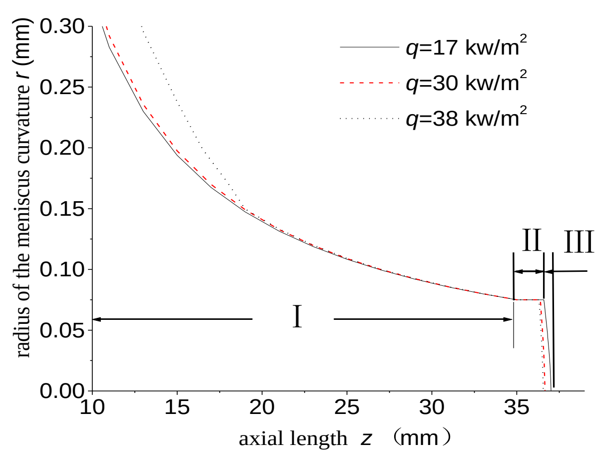

(a) Radius of the meniscus curvature along the groove

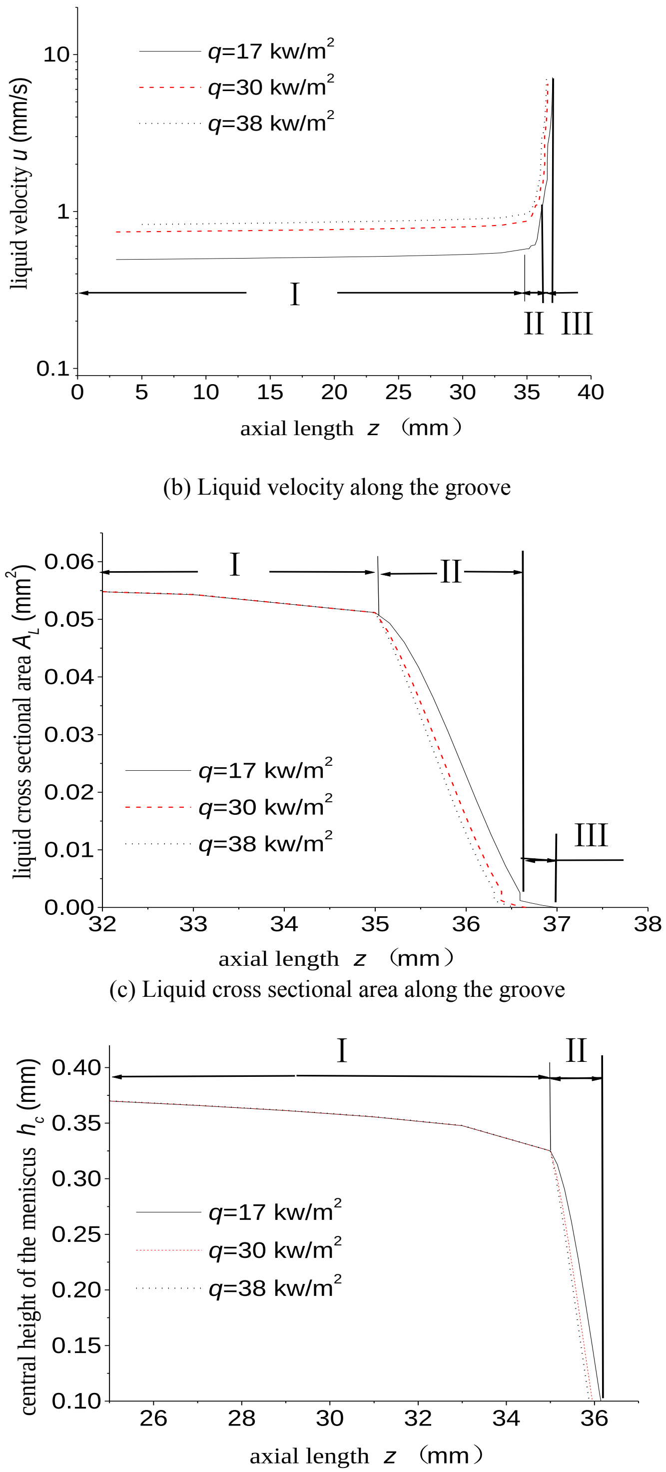

(b) Liquid velocity along the groove

(c) Liquid cross sectional area along the groove

(d) Central height of the meniscus along the groove

Ⅰ accommodation stage; Ⅱ jump-like stage; Ⅲ corner flow stage

Fig.8 Axial flow characteristics along the rectangular microgroove

At the accommodation stage and the corner flow stage, axial change curves of such parameters as radius of the meniscus curvature, liquid velocity, central liquid height, etc. were iteratively calculated by Eq. (3)~(7), Eq. (9), (14), (16) and (17); at the stage of jump-like stage, axial change curves of these parameters were calculated by Eq. (11)~(15). Fig. 8 shows axial flow characteristics in the rectangular microgroove with width of 0.15mm and depth of 0.4mm. As seen in Fig. 8 (a), radius of the meniscus curvature decreases along the groove, and provides capillary force to drive the axial flow; downtrend of the meniscus curvature radius becomes more obvious as the heat load increases; radius of the meniscus curvature drops remarkably at the corner flow stage because the liquid film strongly evaporates in the heating zone, and the axial flow resistance increases greatly. As seen in Fig. 8 (b), axial velocity of the liquid increases as the heat load increases, the main reason is that larger mass flow rate is needed for higher heat load; the liquid velocity increases along the groove, and rapidly rises at the stage of the jump-like transition and the corner flow stage because of reduced cross sectional area for liquid flow. As seen in Fig. 8 (c), the liquid cross sectional area decreases along the groove and it significantly shrinks at the jump-like stage and the corner flow stage; the liquid cross sectional area becomes smaller for higher heat load because stronger evaporation of the liquid is caused. As shown in Fig. 8 (d), the central liquid height decreases along the groove; as the heat load increases, the central liquid height gradually decreases. Fig. 8 shows that at the stage of the jump-like transition and the corner flow stage, flow parameters change significantly but not show the step change, so the dead zone and the step change don’t exist in fact. In order to clarify the mechanism of the axial flow and heat transfer in rectangular microgrooves, further accurate experimental investigations are needed to promote the theoretical analyses.

CONCLUSIONS

The liquid height profile was studied through experimental and theoretical investigations; the meniscus receding process at the jump-like stage was originally analyzed in the paper. The conclusions are as follows:

（1） The accommodation stage is verified by experimental observations, the meniscus remains attached to the upper corners of the groove at this stage. Calculated length of the accommodation stage is smaller than the experimental result when the groove width is large relatively, so the meniscus may not remain circular and maybe becomes in shape of parabola or ellipse. Further observations are needed to analyze the meniscus deformation.

（2） The dead zone and the step change after the accommodation stage don’t exist, but a jump-like transition occurs with the meniscus remarkably receding.

（3） The liquid height profile on the side wall is approximately of a cubic polynomial form in the transition from the accommodation stage to the bottom corner-flow stage according to the experimental results. Calculated axial change curves of flow parameters, such as radius of the meniscus curvature, liquid velocity, liquid height, etc., show that flow characteristics changes significantly at the jump-like stage and the corner flow stage.

（4） The accommodation theory is referred in present paper. In order to verify theoretical analyses introduced in the paper and clarify mechanism of the axial flow in rectangular microgrooves, much more accurate experimental data need to be supplied.

approach for very small tilt angles [J]. ASME J. Heat Transfer, 1998, 120:452-457

ACKNOWLEDGMENTS:

The authors acknowledge the financial support provided by the National Science Foundation of China (Grant No. 50806075).

REFERENCE：

[1] STEPHAN P C, BUSSE C A. Analysis of the heat transfer coefficient of grooved heat pipe evaporator walls [J]. Int. J. Heat Mass Transfer, 1992, 35 (2):383-391

[2] KOBAYASHI Y, TOYOKAWA S, ARAKI T. Heat and mass transfer from thin liquid film in the vicinity of the interline of meniscus [J]. Thermal Science & Engineering, 1994, 2(1): 45-51

[3] KHRUSTALEV D, FAGHRI A. Heat transfer during evaporation on capillary-grooved structures of heat pipes [J]. ASME J. Heat Transfer, 1995, 117: 740-747

[4] XU X, CAREY V P. Film evaporation heat transfer model and its comparison with experimental data [J]. J Thermo-physics, 1990, 4 (4): 512-520

[5] JIAO A. J, MA H. B, CRITSER J. K. Evaporation heat transfer characteristics of a grooved heat pipe with micro-trapezoidal grooves [J]. International Journal of Heat and Mass Transfer, 2007, 50: 2905-2911

[6] AYYASWAMY P S, CATTON I, EDWARDS D K. Capillary flow in triangular grooves [J]. J. Applied Mechanics, 1974, 41: 332-336

[7] HA J M, PETERSON G P. Analytical prediction of the axial dryout point for evaporating liquids in triangular micro grooves [J]. ASME J. Heat Transfer, 1994, 116:498-503

[8] HA J M, PETERSON G P. Capillary performance of evaporating flow in the micro grooves: an analytical approach for very small tilt angles [J]. ASME J. Heat Transfer, 1998, 120:452-457

[9] HA J M, PETERSON G P. Capillary performance of evaporating flow in the micro grooves: an approximate analytical approach and experimental investigation [J]. J. Heat Transfer, 1998, 120:743-750

[10] PETERSON G P, HA J M. The interline heat transfer of evaporation thin films along a micro grooved surface [J]. J. Heat Transfer, 1996, 118:747-754

[11] CATTON I, STROES G. A semi analytical model to predict the capillary limit of heated inclined triangular capillary grooves [J]. ASME J. Heat Transfer, 2002, 124: 162-168

[12] HU XUEGONG, TANG DAWEI. Dryout characteristics of evaporating liquid in vertical capillary microgrooves heat sink [J]. Journal of Chemical Industry and Engineering, 2007, 58 (3): 575-580 (in Chinese)

[13] HU XUEGONG, BAI LI, et al. Theoretical analysis of axial dryout point height in vertical rectangular capillary microgrooves [J]. Journal of China University of Petroleum , 2007,31(3):119-123 (in Chinese)

[14] R. H. NILSON, S. W. TCHIKANDA, S. K. GRIFFITHS, et al. Steady evaporating flow in rectangular microchannels [J]. Int. J. Heat and Mass Transfer, 2006 (49):1603-0618

[15] STROES G, CATTON I. A semi analytical model to predict the dryout point in inclined rectangular channels heated from below [C]. Proceedings of the 11th international heat transfer conference, Kyongju, Korea, 1998, 2:133-138

[16] S. W. TCHIKANDA, R. H. NILSON, S. K. GRIFFITHS. Modeling of pressure and shear driven flows in open rectangular microchannels [J]. Int. J. Heat Mass Transfer, 2004 (47): 527-538